7298 *Inorg. Chem.* **2010**, *49*, 7298–7303
DOI: 10.1021/ic902419z

Inorganic Chemistry
Article

Photophysical Characterization of the Interactions among Tris(2,2′-bipyridyl)ruthenium(II) Complexes Ion-Exchanged within Zirconium Phosphate

Angel A. Martí[⊥] and Jorge L. Colón*[,†]

[†]*Department of Chemistry, P.O. Box 23346, University of Puerto Rico, Río Piedras, Puerto Rico 00931, and* [⊥]*Department of Chemistry, Rice University, 6100 S Main Street, MS-60, Houston, Texas 77005*

Received December 5, 2009

We studied the structures, luminescence, and self-quenching properties of tris(2,2′-bipyridyl)ruthenium(II) ($Ru(bpy)_3^{2+}$) two-dimensional arrangements within the layers of zirconium phosphate (ZrP). The intercalation of $Ru(bpy)_3^{2+}$ was accomplished using a hydrated form of zirconium phosphate ZrP. Varying the $Ru(bpy)_3^{2+}$/ZrP intercalation ratio, different $Ru(bpy)_3^{2+}$-exchanged ZrP loading levels were achieved. The ion exchange of $Ru(bpy)_3^{2+}$ within ZrP produces a red shift in the metal-to-ligand charge-transfer (MLCT) absorption band of the complex from 452 nm in aqueous solution to 460 nm in ZrP. Steady state luminescence spectra of the $Ru(bpy)_3^{2+}$-exchanged ZrP materials show an increase in the luminescence intensity with an increase in the $Ru(bpy)_3^{2+}$ loading level until about 0.77 M, where subsequent increases in the loading level produce a decrease in the luminescence (self-quenching region). Time-resolved luminescence measurements are consistent with the steady state luminescence measurements. Analysis of the time domain luminescence measurements in loadings higher than 0.77 M leads to the determination of a collisional quenching rate constant of $(1.67 \pm 0.05) \times 10^6\ M^{-1}\ s^{-1}$. Stern−Volmer analysis of the luminescence quantum yield of $Ru(bpy)_3^{2+}$-exchanged ZrP materials indicates that static quenching is also involved in the $Ru(bpy)_3^{2+}$ self-quenching mechanism. The quantum yield data behavior might be explained by a model that takes into account collisional quenching and the quasi-static Perrin mechanism. The calculation yields a quenching sphere of action of 14.8 Å, which is slightly larger than the collisional radii of two $Ru(bpy)_3^{2+}$ ions (12.2 Å), as predicted by the model.

Introduction

The immobilization of luminescent metal complexes in rigid matrixes has become an intense area of investigation in the past few years because of its application in solar energy conversion, LED displays, and oxygen sensing, among others.[1−5] Matrixes like zeolites,[6−8] gels,[9] clays,[10] and micelles[11] have been used to immobilize metal complexes resulting in interesting photophysical characteristics. One of the main goals of our research is to develop photoactive materials capable of undergoing artificial photosynthesis, converting solar energy into a more usable form such as electrical or chemical energy. The fabrication of materials utilizing two-dimensional arrays of metal complexes can provide a way of performing artificial photosynthesis; however, this approach requires a deep understanding of the photophysical properties of these photoactive species in well-defined two-dimensional lattices.

We have selected tris(2,2′-bipyridyl)ruthenium(II) ($Ru(bpy)_3^{2+}$) as a model molecule to conduct our experiments, because of its widespread usage and its well-characterized photophysics. In a previous publication we reported the direct intercalation of $Ru(bpy)_3^{2+}$ within the two-dimensional framework of a α-zirconium phosphate (α-ZrP) like material.[12] α-zirconium phosphate ($Zr(HPO_4)_2 \cdot H_2O$, α-ZrP) is a layered inorganic cation exchanger composed of zirconium atoms arranged in a quasi-planar configuration joined by phosphate groups above and below the mean plane of the Zr atoms.[13,14] Three of the oxygens in the phosphate groups are

*To whom correspondence should be addressed. E-mail: jlcolon@uprrp.edu. Phone: (787) 764-0000, ext. 2371. Fax: (787) 756-8242.

(1) Kim, Y.; Lee, H.; Dutta, P. K.; Das, A. *Inorg. Chem.* **2003**, *42*, 4215–4222.
(2) Ogawa, M.; Nakamura, T.; Mori, J.; Kuroda, K. J. *J. Phys. Chem. B* **2000**, *104*, 8554–8556.
(3) Sykora, M.; Kincaid, J. R. *Nature* **1997**, *387*, 162–164.
(4) Nakato, T.; Sakamoto, D.; Kuroda, K.; Kato, C. *Bull. Chem. Soc. Jpn.* **1992**, *65*, 322–328.
(5) Kamat, P. V.; Gopidas, K. R.; Mukherjee, T.; Joshi, V.; Kotkar, D.; Pathak, V. S.; Ghosh, P. K. *J. Phys. Chem.* **1991**, *95*, 10009–10018.
(6) Coutant, M. A.; Le, T.; Castagnola, N.; Dutta, P. K. *J. Phys. Chem. B* **2000**, *104*, 10783–10788.
(7) Vaidyalingam, A.; Dutta, P. K. *Anal. Chem.* **2000**, *72*, 5219–5224.
(8) Castagnola, N.; Dutta, P. K. *J. Phys. Chem. B* **2001**, *105*, 1537–1542.
(9) Matsui, K.; Momose, F. *Chem. Mater.* **1997**, *9*, 2588–2591.
(10) Hagerman, M. E.; Salamone, S. J.; Herbst, R. W.; Payeur, A. L. *Chem. Mater.* **2003**, *15*, 443–450.
(11) Kunjappu, J. T.; Somasundaran, P.; Turro, N. J. *J. Phys. Chem.* **1990**, *94*, 8464–8468.
(12) Martí, A. A.; Colón, J. L. *Inorg. Chem.* **2003**, *42*, 2830–2832.
(13) Troup, J. M.; Clearfield, A. *Inorg. Chem.* **1977**, *16*, 3311–3314.
(14) Clearfield, A.; Smith, G. D. *Inorg. Chem.* **1969**, *8*, 431–436.

 Published on Web 07/19/2010

bonded to three different zirconium atoms in the plane, while the remaining oxygen is bonded to a hydrogen atom and points directly to the interlamellar space. This hydrogen can be ion-exchanged by small cations (< 2.63 Å diameter).[15]

The intercalation of $Ru(bpy)_3^{2+}$ in α-ZrP has been the focus of intense research during the last 30 years. Different methods have been employed to achieve intercalation of $Ru(bpy)_3^{2+}$ within ZrP and to characterize the resulting materials. The first attempt to intercalate $Ru(bpy)_3^{2+}$ in α-ZrP was performed by Yates and co-workers in 1981.[16] These authors achieved the intercalation of $Ru(bpy)_3^{2+}$ within ZrP by carrying out the synthesis of the α-ZrP material in a refluxing $Ru(bpy)_3^{2+}$ solution. The result was an intercalated phase with an interlayer distance of 15.9 Å.[16] Later, Vliers and co-workers spectroscopically characterized $Ru(bpy)_3^{2+}$ intercalated within ZrP by the reflux method (Yates's method) and using direct precipitation in the presence of hydrofluoric acid (HF).[17] The results suggested that the reflux method favored the decomposition of $Ru(bpy)_3^{2+}$ in the interlayer space by protonation of one of its bipyridines. The materials synthesized by direct precipitation with HF resulted in better crystallinity, and no protonation of the bipyridines was observed. In a different approach, Vliers and co-workers intercalated $Ru(bpy)_3^{2+}$ by ion-exchange with hexylamine intercalated ZrP (preintercalation method).[18] The result was a phase with low crystallinity and an interlayer distance of 16.3 Å. Furthermore, Kumar and Williams used α-ZrP preswelled with *n*-butylamine to intercalate $Ru(bpy)_3^{2+}$ within the layers of ZrP, increasing the interlayer distance from 18.6 in *n*-butylamine-intercalated ZrP to 19.5 Å.[19,20] Recently, Wang and co-workers incorporated $Ru(bpy)_3^{2+}$ within ZrP using a layer-by-layer method and demonstrated its possible application as an oxygen sensor.[21] Although some luminescence and time-resolved luminescence spectroscopic characterization has been performed in ZrP materials intercalated with $Ru(bpy)_3^{2+}$ in the presence of pre-swelling agents like butylamine, no studies have been targeted to elucidate the quenching mechanisms operating in $Ru(bpy)_3^{2+}$ intercalated ZrP materials free of anchoring species. These kinds of studies are important since pre-intercalated anchoring species can affect the interaction between $Ru(bpy)_3^{2+}$ complexes within the layers of ZrP.

We previously reported the first direct intercalation of $Ru(bpy)_3^{2+}$ into a ZrP framework without the use of a pre-intercalated anchoring group.[12] Instead of using the previously employed methods, we decided to directly ion-exchange $Ru(bpy)_3^{2+}$ in an α-ZrP-like material consisting of a highly hydrated phase of ZrP that has an enlarged interlayer distance of 10.3 Å.[15,22] The advantage of using the highly hydrated 10.3 Å-ZrP is that it avoids more aggressive synthetic methods that can decompose the $Ru(bpy)_3^{2+}$ complex.[17] This method also avoided the use of pre-swelling species which can remain co-intercalated together with $Ru(bpy)_3^{2+}$ in the interlayer space, changing the properties of the layer's microenvironment and subsequently those of the metal complex.[18−20] This new method also allows the easy preparation of materials with different $Ru(bpy)_3^{2+}$ loadings, allowing the study of the photophysical properties of $Ru(bpy)_3^{2+}$ in a two-dimensional arrangement, where the distance between metal complexes can be modulated.[12]

Table 1. Composition of the Different $Ru(bpy)_3^{2+}$-Exchanged ZrP Loadings Determined by Elemental Analysis and TGA Measurements

$Ru(bpy)_3^{2+}$/ZrP intercalation ratio	$Ru(bpy)_3^{2+}$-exchanged ZrP loading (mol/dm^3)	$Zr(H_{1-2n}PO_4)_2(Ru(bpy)_3^{2+})_{2n}\cdot 2mH_2O$ [a]	
		n	*m*
5:1	0.86	0.093	1.49
1:1	0.81	0.088	1.49
1:5	0.80	0.087	1.45
1:10	0.79	0.086	1.53
1:12	0.77	0.084	1.55
1:15	0.60	0.064	1.46
1:17	0.49	0.052	1.36
1:20	0.43	0.046	1.33
1:20	0.30	0.032	1.12
1:30	0.25	0.026	1.03

[a] The formula assumes a pure phase.

In this paper, we present the photophysical characterization of the interaction among $Ru(bpy)_3^{2+}$ molecules intercalated in the ZrP lamellar lattice. On the basis of structural and theoretical considerations, we present a proposed structure orientation for the arrangement of the $Ru(bpy)_3^{2+}$ molecules within the layers of ZrP. Furthermore, steady-state and time-resolved luminescence spectroscopies were used to characterize the exchanged material, including the elucidation of its self-quenching mechanism.

Experimental Section

Materials. All chemicals were purchased from Aldrich Chemical Co. and used as received with the exception of phosphoric acid, 85% (v/v) (H_3PO_4), which was purchased from Fisher.

Intercalation Experiments. The synthesis of 10.3 Å-ZrP[23] and the intercalation of $Ru(bpy)_3^{2+}$ within 10.3 Å-ZrP are reported elsewhere.[12] Different loading levels of $Ru(bpy)_3^{2+}$ within the layers were obtained by changing the $Ru(bpy)_3^{2+}$/ZrP molar ratio in the intercalation mixture as previously reported.[12] The range of $Ru(bpy)_3^{2+}$/ZrP intercalation molar ratios used in our experiments was from 1:30 to 5:1 (Table 1).

Instrumentation. UV−vis absorption measurements were performed on a HP-8453 diode array spectrophotometer using quartz cells (1 cm path length). Luminescence measurements were performed on a SE-900 spectrofluorometer (Photon Technology International, PTI) using a 150 W xenon lamp as the excitation source. The bandpass of the emission monochromator was 6.25 nm. Time-resolved luminescence experiments were performed using an Oriel lifetime spectrometer as described elsewhere.[24] The models used to fit the transients were single exponential and double exponential decays models, using Sigma

(15) Clearfield, A.; Duax, W. L.; Medina, A. S.; Smith, G. D.; Thomas, J. R. *J. Phys. Chem.* **1969**, *73*, 3424–3430.
(16) Yates, R. C.; Kuznicki, S. M.; Lloyd, L. B.; Eyring, E. M. *J. Inorg. Nucl. Chem.* **1981**, *43*, 2355–2358.
(17) Vliers, D. P.; Schoonheydt, R. A.; De Schryver, F. C. *J. Chem. Soc., Faraday Trans.* **1985**, *81*, 2009–2019.
(18) Vliers, D. P.; Collin, D.; Schoonheydt, R. A.; De Schryver, F. C. *Langmuir* **1986**, *2*, 165–169.
(19) Kumar, C. V.; Williams, Z. J. *J. Phys. Chem.* **1995**, *99*, 17632–17639.
(20) Kumar, C. V.; Williams, Z. J.; Turner, R. S. *J. Phys. Chem.* **1998**, *102*, 5562–5568.
(21) Wang, Q.; Yu, D.; Wang, Y.; Sun, J.; Shen, J. *Langmuir* **2008**, *24*, 11684–11690.
(22) Alberti, G.; Costantino, U.; Gill, J. S. *J. Inorg. Nucl. Chem.* **1976**, *38*, 1733–1738.
(23) Kijima, T. *Bull. Chem. Soc. Jpn.* **1982**, *55*, 3031–3032.
(24) Martí, A. A.; Rivera, N.; Soto, K.; Maldonado, L.; Colón, J. L. *J. Chem. Soc., Dalton Trans.* **2007**, 1713–1718.

Plot 8.0 software. The selection of the best fit was determined by minimizing the sum of the square differences between the calculated and the experimental intensities, by the squared correlation coefficient (r^2, best fit closer to 1), by visual inspection of the computed fit and the experimental transient, and by the plot of the residuals versus time (random oscillations around zero are expected for a good fit).[25] The reported error for each lifetime was calculated from the standard deviation of three independent measurements using a student's *t*-test method.

The steady-state and time-resolved luminescence measurements for $Ru(bpy)_3^{2+}$-exchanged ZrP were obtained from dilute suspensions (0.008%, m/v). Prior to the measurements, the suspensions were purged with ultrapure N_2 (99.999%) for 15 min. Quantum yields were determined as described by Vliers et al.[18] using $Ru(bpy)_3Cl_2$ in water ($\phi = 0.042$) as the standard.[26] The integration of the areas under the luminescence curves was obtained with the PTI Felix 1.42b program. The reported error for each quantum yield was calculated from the standard deviation of three independent measurements using a student's *t*-test method.

IR spectra of the intercalated materials were recorded on KBr pellets (1%, w/w) with a Nicolet Magna 750 FTIR spectrometer, while IR spectra of wet and dry 10.3 Å-ZrP were measured directly on the sample with a Bruker Tensor 27 FTIR spectrometer. X-ray powder diffraction (XRPD) experiments were performed from 2 to 45° (in 2θ) using a Siemens D5000 X-ray diffractometer system with a copper anode source (CuK_α, λ = 1.5418 Å). The widths of the slits used were: divergence slit, 2 mm; receiving slit, 2 mm; scatter slit, 0.6 mm; detector slit, 2 mm. The interlayer distance (d_{hkl}) of the ZrP materials was determined from the first order diffraction peak following Bragg's Law.[27]

Thermogravimetric analysis (TGA) was obtained with a Shimadzu Thermogravimetric Analyzer (TGA-50) with a heating rate of 5°/min. Elemental analysis was performed by Quantitative Technologies Inc. (QTI). TGA and elemental analysis results were used to determine the $Ru(bpy)_3^{2+}$ intercalation loading level within ZrP (Table 1 and Table S1, Supporting Information).

Results and Discussion

The ion exchange of $Ru(bpy)_3^{2+}$ within the layers of 10.3 Å-ZrP produced some structural changes in the morphology of the layers that were characterized by different techniques. With the purpose of studying how $Ru(bpy)_3^{2+}$ was affected by its encapsulation in this lamellar material and vice versa, intercalation at different $Ru(bpy)_3^{2+}$/ZrP molar ratios were performed obtaining materials with different loading levels. To determine the amount of $Ru(bpy)_3^{2+}$ intercalated, the sample composition obtained from elemental analysis (Carbon weight percent) and TGA (water weight percent) were studied. The information derived from these analyses is shown in Table 1. The variables *n* and *m* represent the molar amount of $Ru(bpy)_3^{2+}$ and water per cationic site, respectively (for the purpose of this discussion a cationic site is a site in the ZrP lattice where cation exchange can occurs (OPO_3^-); there are two cationic sites per ZrP formula unit).

All intercalated materials show a distinctive diffraction peak at 15.1 Å which is indicative of intercalation and consistent with previous results.[12] It is important to note that the peak at 10.3 Å only exists in the hydrated non-intercalated phase of 10.3 Å-ZrP. This means that for dry materials after the intercalation reaction, what will be seen is the 7.6 Å phase[28] (α-ZrP) if no intercalation occurs, or a 7.6 Å peak will be seen if the intercalation product is a mixed phase with some 7.6 Å phase present. This 7.6 Å peak is very likely overlapped by the second order diffraction peak around 7.4 Å (for 0.25 M material), forming a very broad peak, observable in the XRPD pattern. The similar height of the 7.4 Å peak and the 14.5 Å peak is consistent with this argument, implying that at this concentration both phases (non-intercalated and intercalated) are present. It is likely that mixed phases exist below 0.77 M, as the crystallinity of the material decrease. The XRPD patterns for $Ru(bpy)_3^{2+}$-exchanged ZrP at different loadings levels are presented in the Supporting Information, Figure S1. The maximum loading of $Ru(bpy)_3^{2+}$ within the layers of ZrP was calculated as 0.87 M, by using geometrical considerations described elsewhere.[24,28] The theoretical maximum molarity compares with the value for the maximum loading of 0.86 M obtained experimentally, indicating that a maximum loading level has been achieved.

The IR spectra for different $Ru(bpy)_3^{2+}$-exchanged ZrP loadings are shown in Supporting Information, Figure S4. It is expected that if $Ru(bpy)_3^{2+}$ does not undergo any chemical change after intercalation, the IR spectrum of the $Ru(bpy)_3^{2+}$-exchanged ZrP material should be similar to the sum of the spectra of the ZrP material and the metal complex.[29] The appearance of new peaks or large displacements of the existing ones would indicate changes in the structure of the intercalated molecule or the layered material. The 10.3 Å-ZrP material possesses an IR spectrum very similar to α-ZrP. In the region from 2000 to 400 cm^{-1} some bands characteristic of this layered material can be identified.[30] The band at 1631 cm^{-1} has been identified as belonging to water bending vibrations, since the band is completely absent following dehydration. The phosphate groups give bands around 1038 cm^{-1}, due to orthophosphate vibrations, a band at 1248 cm^{-1}, attributed to the deformation of the P−O−H bond and one at 965 cm^{-1}, corresponding to the phosphate vibrations of the symmetric C_{3v} group. The bands from 600 to 400 cm^{-1} are attributed to phosphate bending motions. In the case of $Ru(bpy)_3^{2+}$-exchanged ZrP, bands at about 1600−1350 cm^{-1}, due to the bipyridine ligand vibrations and some bands assigned to deformation vibrational frequencies in the range between 900 and 700 cm^{-1} are expected. The spectra of the exchanged materials appear to be the sum of spectra due to $Ru(bpy)_3^{2+}$ and the 10.3 Å-ZrP material, with no new peaks or major band displacements (Supporting Information, Figure S4). The most prominent difference is the broadening of the ZrP band at 1038 cm^{-1}, which is expected because of the heterogeneous environment induced as a consequence of $Ru(bpy)_3^{2+}$ intercalation. These results indicate that both $Ru(bpy)_3^{2+}$ and ZrP remain chemically intact following the intercalation process.

The UV−vis absorption spectrum of $Ru(bpy)_3^{2+}$ in aqueous solution shows the metal-to-ligand charge-transfer (MLCT) maximum absorption at about 453 nm. The absorption spectra of $Ru(bpy)_3^{2+}$-exchanged ZrP suspensions show

(25) Lakowicz, J. R. *Principles of Fluorescence Spectroscopy*, 2nd ed.; Kluwer Academics/Plenum Publishers: New York, 1999.
(26) Juris, A.; Balzani, V.; Barigelletti, F.; Campagna, S.; Belser, P.; Zelewsky, V. A. *Coord. Chem. Rev.* **1988**, *84*, 85–277.
(27) Jenkins, R.; Snyder, R. L. *Introduction to X-Ray Powder Diffractometry*; John Wiley and Sons: New York, 1996.
(28) Martí, A. A.; Paralitici, G.; Maldonado, L.; Colón, J. L. *Inorg. Chim. Acta* **2007**, *360*, 1535–1542.
(29) Colón, J. L.; Yang, C.-Y.; Clearfield, A.; Martin, C. R. *J. Phys. Chem.* **1988**, *92*, 5777–5781.
(30) Horsley, S. E.; Nowell, D. V.; Stewart, D. T. *Spectrochim. Acta* **1974**, *30A*, 535–541.

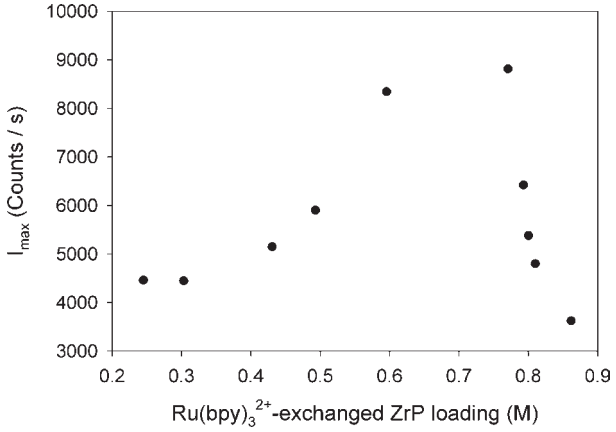

Figure 1. Luminescence intensity at λ_{max} of aqueous suspensions of $Ru(bpy)_3^{2+}$-exchanged ZrP at different loading levels. The concentrations of the suspensions were adjusted to the same absorption on the MLCT band.

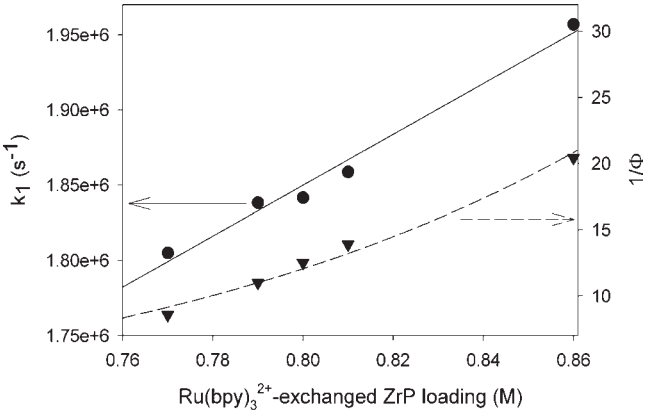

Figure 2. Time-resolved kinetic rate constant (solid dots are the experimental data and the line is the fit to $\tau^{-1} = \tau_0^{-1} + k_q$ [Q]) and reciprocal quantum yields (inverted triangles are the experimental data and the dashed line is the fit to eq 4) as a function of $Ru(bpy)_3^{2+}$-exchanged ZrP loading.

a red shift of the MLCT band of up to 18 nm (Supporting Information, Table S2). Similar displacements have been seen in solution, zeolitic, and layered materials with increasing concentration of $Ru(bpy)_3^{2+}$.[18,29,31−34] This red-shift could be due to the stabilization of the excited state by interaction of $Ru(bpy)_3^{2+}$ with the highly polar ZrP surface, although destabilization of the ground state has also been used to explain these observations.[31] Alternative explanations include the change in the refractive index going from solution to the solid material,[18] and interaction between $Ru(bpy)_3^{2+}$ ions in the materials.[33]

The luminescence spectra of $Ru(bpy)_3^{2+}$-exchanged ZrP materials resemble those observed in aqueous solution, with a slight blue shift of λ_{max} from 597 nm in aqueous solution to 589 nm in the exchanged material. The similarity of the λ_{max} values is indicative of the polar microenvironment experienced by the $Ru(bpy)_3^{2+}$ probes in the interlayer region, which is consistent with the highly hydrated state of the ZrP and with the ionic nature of the lattice.[24] The observed blue shift is in-keeping with the rigidochromic effect because of the more rigid environment in the interlayer region of the exchanged material.[35,36] Furthermore, as $Ru(bpy)_3^{2+}$ loading increases, the amount of water molecules per $Ru(bpy)_3^{2+}$ decreases. This effect is not apparent from Table 1, where the amount of water inside the layer seems to increase with loading. However, the effect of water on $Ru(bpy)_3^{2+}$ must be considered not in relation with the bulk concentration of water in $Ru(bpy)_3^{2+}$-exchanged ZrP (variable m, Table 1) but in relation to the amount of water per $Ru(bpy)_3^{2+}$ ion. This value is obtained from the m/n ratio in Table 1 and is plotted as a function of the $Ru(bpy)_3^{2+}$ loading in the Supporting Information, Figure S5. From this figure, a clear decrease in the amount of water per $Ru(bpy)_3^{2+}$ is observed, which results in less water molecules available to stabilize the excited state dipole and therefore leads to a rise of the emissive state energy. Figure 1 shows the luminescence intensity at λ_{max} as a function of the $Ru(bpy)_3^{2+}$ loading. The increase of the $Ru(bpy)_3^{2+}$ concentration within the layers causes an increase in the observed luminescence up to a point after which subsequent increases in loading lead to a decrease in the luminescence. This effect is consistent with self-quenching of the excited state and will be discussed later in this section.

Luminescence lifetime measurements were also performed for $Ru(bpy)_3^{2+}$-exchanged ZrP. The obtained time-resolved luminescence decay curves were analyzed using single and double exponential decay models. The best fits were obtained for the double exponential decay model, and the results are shown in Table 2. The data show that two components with abundances of about 5 and 95% exist in $Ru(bpy)_3^{2+}$-exchanged ZrP, independently of loading level. This biexponential behavior has previously been observed for $Ru(bpy)_3^{2+}$ in other rigid media.[9,10,33,36] Although the nature of the short and less abundant component is not well understood, one possibility is that it arises from lattice sites where $Ru(bpy)_3^{2+}$ is more strongly quenched. Moreover, it is possible that here the emission dipole moment of some $Ru(bpy)_3^{2+}$ molecules is correctly aligned with P−O−H groups in ZrP, resulting in efficient quenching by energy transfer to the O−H vibrational modes.[36] A plot of the decay rate constant of the longer and more abundant component as a function of the loading shows a linear increase with concentration (Figure 2). For this plot we only considered the materials that gave crystalline phases, since they would have homogeneous and well-defined two-dimensional structures (as seen from Supporting Information, Figure S1, this requirement is fulfilled for materials with loadings larger that 0.77 M). The plot of the decay rate constant of the short component (τ_2) as a function of the $Ru(bpy)_3^{2+}$ loading level shows a random distribution of the lifetimes with no defined tendency (data not shown).

The least-squares fit of the decay rate constants ($1/\tau$) for the slowly decaying lifetime components (Figure 2) yields a straight line with a slope of $(1.69 \pm 0.02) \times 10^6\ M^{-1}\ s^{-1}$. The decrease of the luminescence lifetime with the increase in $Ru(bpy)_3^{2+}$ loading is consistent with a catalyzed deactivation of the excited state through collisions with neighboring ground state $Ru(bpy)_3^{2+}$ complexes.[19,37] The value of the

(31) DellaGuardia, R. A.; Thomas, J. R. *J. Phys. Chem.* **1983**, *87*, 990–998.
(32) Colón, J. L. Doctoral Dissertation, Texas A&M University, College Station, TX, 1989.
(33) Turbeville, W.; Robins, D. S.; Dutta, P. K. *J. Phys. Chem.* **1992**, *96*, 5024–5029.
(34) Schoonheydt, R. A.; De Pauw, P.; Vliers, D. P.; De Schrijver, F. C. *J. Phys. Chem.* **1984**, *88*, 5113–5118.
(35) Wrighton, M.; Morse, D. L. *J. Am. Chem. Soc.* **1974**, *96*, 998–1003.
(36) Innocenzi, P.; Kozuka, H.; Yoko, T. *J. Phys. Chem. B* **1997**, *101*, 2285–2291.
(37) Colón, J. L.; Yang, C.-Y.; Clearfield, A.; Martin, C. R. *J. Phys. Chem.* **1990**, *94*, 874–882.

Table 2. Excited State Lifetimes and Derived Parameters for $Ru(bpy)_3^{2+}$-Exchanged ZrP Suspensions

$Ru(bpy)_3^{2+}$ loading (M)	τ_1, ns[a] (abundance, %)	τ_2, ns[b] (abundance, %)	root mean square displacement of $Ru(bpy)_3^{2+}$ (Å)	collisional distance of $Ru(bpy)_3^{2+}$ (Å)
0.86	511 (94)	64 (6)	3.04	1.3
0.81	538 (95)	71 (5)	3.12	2.0
0.80	543 (95)	71 (5)	3.13	2.1
0.79	544 (96)	67 (4)	3.14	2.3
0.77	554 (96)	63 (4)	3.17	2.7
0.60	542 (96)	60 (4)	3.13	6.6
0.49	559 (95)	71 (5)	3.18	9.8
0.43	537 (95)	62 (5)	3.12	19.6
0.30	559 (96)	63 (4)	3.18	12.0
0.25	546 (96)	53 (4)	3.14	24.4

[a] ±6 ns. [b] ±5 ns.

slope in this plot (1.69×10^6 M^{-1} s^{-1}) is also called k_q and is the self-quenching bimolecular rate constant for the complex in this material. This value is nearly two times larger than the 7.0×10^5 M^{-1} s^{-1} value obtained for $Ru(bpy)_3^{2+}$ in ZrPS by Colón et al.[37] Assuming that each collision results in quenching, then the quenching rate constant (k_q) is equal to the collisional frequency rate constant (k_0) and is related to the diffusion of the molecules by the Smolouchowski equation:

$$k_q = k_0 = \frac{4\pi N_{av}}{1000}(R_l + R_Q)(D_l + D_Q) \quad (1)$$

where, R_l and R_Q are the collision radii of the luminophore and the quencher, respectively, D_l and D_Q are the diffusion coefficients of the luminophore and the quencher, respectively, and N_{av} is Avogadro's number. Using the determined k_q constant, this equation allows to determine a diffusion coefficient for the movement of $Ru(bpy)_3^{2+}$ within the ZrP layers of 9.1×10^{-10} cm^2/s. This diffusion coefficient value compares with previous values observed in ZrPS[37] and polysiloxane films[38] of 6.62×10^{-10} cm^2/s and 3.8×10^{-10} cm^2/s, respectively.

Making use of this diffusion coefficient it is possible to calculate the root-mean-square distance traveled by a $Ru(bpy)_3^{2+*}$ cation in a defined time interval (t) using the Einstein−Smoluchowski equation:[39]

$$\Delta x_{rms} = \langle(\Delta x)^2\rangle^{1/2} = \sqrt{2Dt} \quad (2)$$

where, Δx_{rms} is the square root of the squared mean displacement. Using eq 2, the root-mean-square displacements during the excited state at every loading level were determined (Table 2). The amount of cationic sites available per $Ru(bpy)_3^{2+}$ ion are known (Table 1), and because each cationic site in ZrP possesses an area of about 12 $Å^2$ (2 cationic sites in 24 $Å^2$ when projected in one *ab* plane) the approximate $Ru(bpy)_3^{2+}$ collision distances at different loadings were determined using the following equation:

$$d(Å) = 2\sqrt{\frac{12\ Å^2}{n \times \pi}} - 12.2\ Å \quad (3)$$

where, n is the number of $Ru(bpy)_3^{2+}$ ions per cationic sites (Table 1) and 12.2 Å is the diameter of the cross-sectional area of $Ru(bpy)_3^{2+}$.[40] The results are summarized in Table 2. The data indicates that for all the loadings larger than 0.77 M there is a high probability that an excited $Ru(bpy)_3^{2+}$ will collide with another $Ru(bpy)_3^{2+}$ in its ground state; this is because the translational movement of an excited $Ru(bpy)_3^{2+}$ is shorter than the intermolecular $Ru(bpy)_3^{2+}$ distance in materials with loading larger than 0.77 M. In contrast, the collisional distance for all the loadings from 0.60 M and less are smaller than the root mean displacements of $Ru(bpy)_3^{2+}$ in the excited state, which inhibits the collision or interaction of an excited $Ru(bpy)_3^{2+}$ with another $Ru(bpy)_3^{2+}$ during its excited state lifetime.

Although the proposed model is consistent with the observed lifetimes, full characterization of the quenching mechanism of this inorganic assembly needs the evaluation of steady-state luminescence data. As mentioned previously, the steady-state luminescence measurements are consistent with the occurrence of a self-quenching mechanism. Although the intensity of the luminescence peaks is generally used to evaluate quenching parameters through Stern−Volmer analyses,[25] this procedure is not applicable in this case. The reason being that the luminescence of $Ru(bpy)_3^{2+}$ in suspensions depends on the total suspension concentration of $Ru(bpy)_3^{2+}$-exchanged ZrP materials and in the $Ru(bpy)_3^{2+}$ loading in the material. Because all the $Ru(bpy)_3^{2+}$-exchanged ZrP materials at different loadings levels possess different amounts of probe molecules, it is difficult to correlate the luminescence intensity of the suspensions with the concentration of $Ru(bpy)_3^{2+}$. An alternate way to perform the Stern−Volmer analysis is to use the luminescence quantum yields (Φ) instead of the luminescence intensities.[41] The quantum yields will only depend on the loading of the material and not on the suspension concentration. Table 3 shows the quantum yields determined for the different $Ru(bpy)_3^{2+}$-exchanged ZrP loadings.

The plot of the reciprocal of the quantum yield as a function of $Ru(bpy)_3^{2+}$ loading indicates non-classical Stern−Volmer behavior (Figure 2). Notwithstanding similarities of the plots in Figure 2, which are consistent with the occurrence of a collisional deactivation mechanism, the final assignment requires the correspondence of the Stern−Volmer constants of both the quantum yield and the lifetime measurements. The Stern−Volmer constants can be calculated by multiplying $k_q \times \tau_0$ for the lifetime plot and the slope of the Φ_0/Φ plot for

(38) Nagai, K.; Ueno, Y.; Takamiya, N. *Macromol. Chem. Phys.* **1995**, *196*, 1241–1250.

(39) Einstein, A. In *Einstein's Miraculous Year*; Stachel, J., Ed.; Princeton University Press: Princeton, NJ, 1998; pp 85−98.

(40) The area occupied by a $Ru(bpy)_3^{2+}$ cation projected over one *ab* plane is 12 $Å^2/n$. Then, the distance between the centers of two $Ru(bpy)_3^{2+}$ cations is described by the expression $(12\ Å^2/n) = \pi(d/2)^2$ or $d = 2\sqrt{12/(n\pi)}$. The distance between the corners of two $Ru(bpy)_3^{2+}$ cations is the calculated d, minus two times the radius of $Ru(bpy)_3^{2+}$(12.2 Å). This leads to the collisional distances between two $Ru(bpy)_3^{2+}$ in the ZrP materials.

(41) Turro, N. J. *Modern Molecular Photochemistry*; University Science Books: Mill Valley, CA, 1991; pp 4−6.

Table 3. Luminescence Quantum Yield at Different $Ru(bpy)_3^{2+}$ Loading Levels

$Ru(bpy)_3^{2+}$ loading (M)	quantum yield[a]
0.86	0.049
0.81	0.072
0.80	0.080
0.79	0.091
0.77	0.117
0.60	0.123
0.49	0.108
0.43	0.115
0.30	0.115
0.25	0.098

[a] Approximate error of ±5%.

the quantum yields (since it is difficult to assess the values of τ_0 and Φ_0, we used the values where the lowest quenching occurred as an approximation, i.e., those at 0.77 M based on lifetime measurements). The calculated Stern−Volmer K_D constants are 0.92 M^{-1} from lifetime measurements, and 16.96 M^{-1} from quantum yield measurements. The K_D constants differ by a factor of 20, which is indicative of a static quenching contribution to the total luminescence deactivation pathway.

The most basic mechanism of static quenching is ground-state complex formation.[25] However, UV−vis absorption spectra did not show any evidence of ground state complex formation. A more plausible quenching mechanism is the Perrin model, which states that if the luminophore is in a high quencher concentration environment, the probability of finding a quencher adjacent to it is large, and its luminescence can be quenched instantaneously.[42] This type of quasi-static mechanism is based in the occurrence of a sphere-of-action, which is the distance range where a luminophore is deactivated by a quencher with an efficiency of 1. The form of Perrin's equation used to fit quantum yield data in the quenching region was arranged as

$$\frac{1}{\Phi} = \frac{(1+K_D[Q])e^{[Q]V}}{\Phi_0} \qquad (4)$$

where, V is the sphere-of-action volume with units of L/mol and $K_D = 0.9193\ M^{-1}$ from Stern−Volmer analysis of the luminescence time-resolved data. The results are shown in Figure 2. The fit obtained for this equation allows the calculation of a sphere-of-action volume of $8.4 \pm 0.6\ M^{-1}$. This value corresponds to a sphere-of-action radius of 14.8 Å. This distance is slightly larger than the sum of two $Ru(bpy)_3^{2+}$ radii (12.2 Å) leaving a collision distance of 2.55 Å. The value of 2.55 Å is smaller that the kinetic diameter of a water molecule (3.9 Å) which indicates that two $Ru(bpy)_3^{2+}$ molecules at this distance are within the first solvent shell of each other. This is consistent with the value obtained by Turbeville et al. of 13 Å for $Ru(bpy)_3^{2+}$ in zeolites.[33] This data seems to indicate that if the $Ru(bpy)_3^{2+}$ loading is high enough to allow the population of the first solvent shell with one or more $Ru(bpy)_3^{2+}$ ions, a Perrin's excited state deactivation mechanism may be invoked.

(42) Yguerabide, J.; Yguerabide, E. E. In *Optical Techniques in Biological Research*; Rousseau, D. L., Ed.; Academic Press: New York, 1994; pp 181−289.

Conclusion

In summary, we have photophysically characterized the interactions of $Ru(bpy)_3^{2+}$ within the layers of 10.3 Å-ZrP. The ZrP interlayer distance was increased from 10.3 Å up to 15.1 Å upon intercalation with the $Ru(bpy)_3^{2+}$ complex. Analysis of the data indicates that the $Ru(bpy)_3^{2+}$/ZrP molar intercalation ratio allows the achievement of full loading of $Ru(bpy)_3^{2+}$ in the exchanged material. FT-IR experiments confirm that the intercalation of $Ru(bpy)_3^{2+}$ does not affect significantly its structure or the structure of the ZrP layers.

The intercalation of $Ru(bpy)_3^{2+}$ within the layers of ZrP influences its photophysical properties. Red shifts of the MLCT absorption bands of up to 18 nm were observed in the intercalated material in comparison to $Ru(bpy)_3^{2+}$ ions in solution. A slight blue shift of the luminescence band is also observed which can be explained by the rigid environment that $Ru(bpy)_3^{2+}$ senses within the layers (rigidochromic effect). The lifetime and quantum yield data indicate that the deactivation of $Ru(bpy)_3^{2+}$ is highly dependent on the loading. From a loading of 0.77 M, the quantum yield and the lifetime decreased with increasing loading. This effect is attributed to self-quenching of the emissive excited state. Two mechanisms, collisional and Perrin's, were proposed to be responsible for the self-quenching. The collisional mechanism can be fitted to a linear Stern−Volmer model, giving a quenching constant of $(1.67 \pm 0.05) \times 10^6\ M^{-1}\ s^{-1}$. The quasi-static mechanism was found to comply with a Perrin's mechanism, with a sphere-of-action of 14.76 Å. Both mechanisms are consistent with the lifetime and quantum yield data. The mathematical analysis leads to the conclusion that if the $Ru(bpy)_3^{2+}$ concentration is high enough, the probability that $Ru(bpy)_3^{2+}$ can be within the solvation shell of another $Ru(bpy)_3^{2+}$ ion is high and quenching occurs.

Acknowledgment. We thank Dr. Raphael Raptis for helpful discussions and NIH-RISE (Grant R25GM061151) for financial support.

Supporting Information Available: Carbon elemental analysis and TGA data, XRPD patters, spectra and tabular values of λ_{max} of the UV−vis absorption MLCT band and luminescence spectra for $Ru(bpy)_3^{2+}$-exchanged ZrP, IR spectra of $Ru(bpy)_3^{2+}$-exchanged ZrP materials, and graphical representation of the amount of water per $Ru(bpy)_3^{2+}$ molecule in ZrP. This material is available free of charge via the Internet at http://pubs.acs.org.